

Chapter 3

Overview of the Experimental Technique

In this chapter we give an overview of how the experiment is done. This is followed by a number of chapters that give the details of the specific hardware being developed for E989. The order of those chapters follows the WBS as closely as possible.

The experiment consists of the following steps:

1. Production of an appropriate pulsed proton beam by an accelerator complex.
2. Production of pions using the proton beam that has been prepared.
3. Collection of polarized muons from pion decay $\pi^+ \rightarrow \mu^+ \nu_\mu$
4. Transporting the muon beam to the $(g - 2)$ storage ring.
5. Injection of the muon beam into the storage ring.
6. Kicking the muon beam onto stored orbits.
7. Measuring the arrival time and energy of positrons from the decay $\mu^+ \rightarrow e^+ \bar{\nu}_\mu \nu_e$
8. Precise mapping and monitoring of the precision magnetic field

Central to the determination of a_μ is the spin equation¹

$$\vec{\omega}_a = -\frac{Qe}{m} \left[a\vec{B} - \left(a - \frac{1}{\gamma^2 - 1} \right) \frac{\vec{\beta} \times \vec{E}}{c} \right] = -\frac{Qe}{m} \left[a_\mu \vec{B} - \left(a_\mu - \left(\frac{mc}{p} \right)^2 \right) \frac{\vec{\beta} \times \vec{E}}{c} \right], \quad (3.1)$$

that gives the rate at which the muon spin turns relative the momentum vector, which turns with the cyclotron frequency. The electric field term is there since we use electrostatic vertical focusing in the ring. At the magic momentum, $p_m = 3.09$ GeV/c, the effect of the motional magnetic field (the $\vec{\beta} \times \vec{E}$ term) vanishes.

Measurement of a_μ requires the determination of the muon spin frequency ω_a and the magnetic field \vec{B} averaged over the muon distribution.

¹See Section 3.3 for the details.

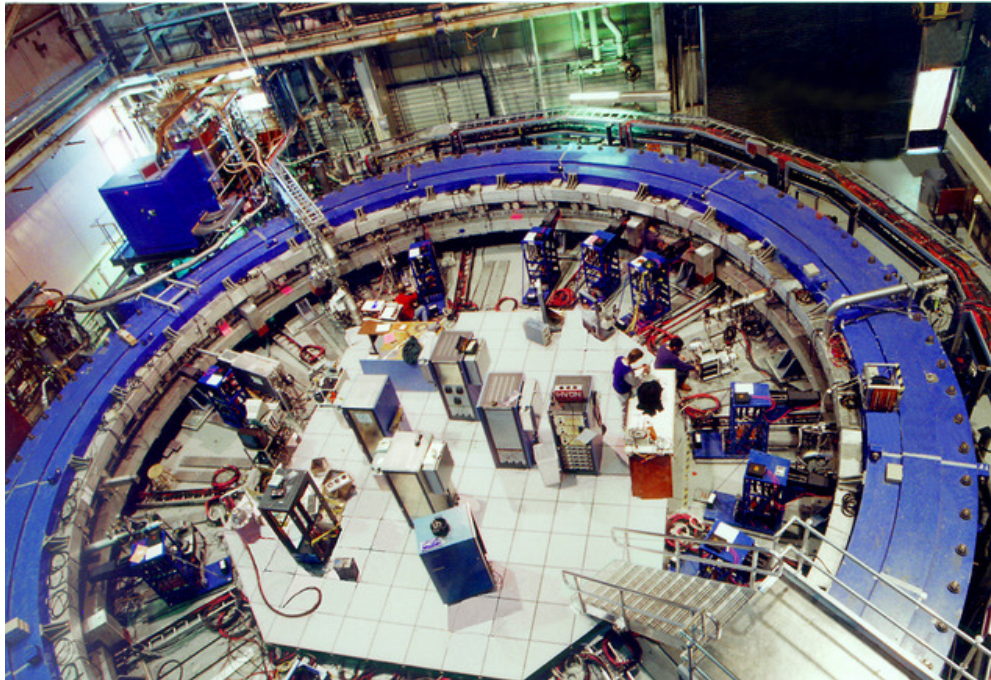


Figure 3.1: The E821 storage-ring magnet at Brookhaven Lab.

3.1 Production and Preparation of the Muon Beam

E989 will bring a bunched beam from the 8 GeV Booster to a pion production target located where the antiproton production target was in the Tevatron collider program (see Chapter 7). Pions of $3.11 \text{ GeV}/c \pm 5\%$ will be collected and sent into a large-acceptance beamline. Muons are produced in the weak pion decay

$$\pi^\mp \rightarrow \mu^\mp + \bar{\nu}_\mu(\nu_\mu). \quad (3.2)$$

The antineutrino (neutrino) is right-handed (left-handed) and the pion is spin zero. Thus the muon spin must be antiparallel to the neutrino spin, so it is also right-handed (left-handed). A beam of polarized muons can be obtained from a beam of pions by selecting the highest-energy muons (a “forward beam”) or by selecting the lowest-energy muons (a “backward beam”), where forward or backward refers to whether the decay is forward or backward in the center-of-mass frame relative to the pion momentum. Polarizations significantly greater than 90% are easily obtained in such beams. The pions and daughter muons will be injected into the Delivery Ring (the re-purposed \bar{p} debuncher ring), where after several turns the remaining pions decay. The surviving muon beam will be extracted and brought to the muon storage ring built for E821 at Brookhaven.

3.2 Injection into the Storage Ring

A photograph of the E821 magnet is shown in Figure 3.1. It is clear from the photo that this “storage ring” is very different from the usual one that consists of lumped elements. The

storage ring magnet is energized by three superconducting coils shown in Fig 3.2(b). The continuous “C” magnet yoke is built from twelve 30° segments of iron, which were designed to eliminate the end effects present in lumped magnets. This construction eliminates the large gradients that would make the determination of the average magnetic field, $\langle B \rangle$, very difficult. Furthermore, a small perturbation in the yoke can effect the field at the ppm level at the opposite side of the ring. Thus every effort is made to minimize holes in the yoke, and other perturbations. The only penetrations through the yoke are to permit the muon beam to enter the magnet as shown in Fig 3.2(a), and to connect cryogenic services and power to the inflector magnet and to the outer radius coil (see Fig. 3.2(b)). Where a hole in the yoke is necessary, extra steel was placed around the hole on the outside of the yoke to compensate for the missing material.

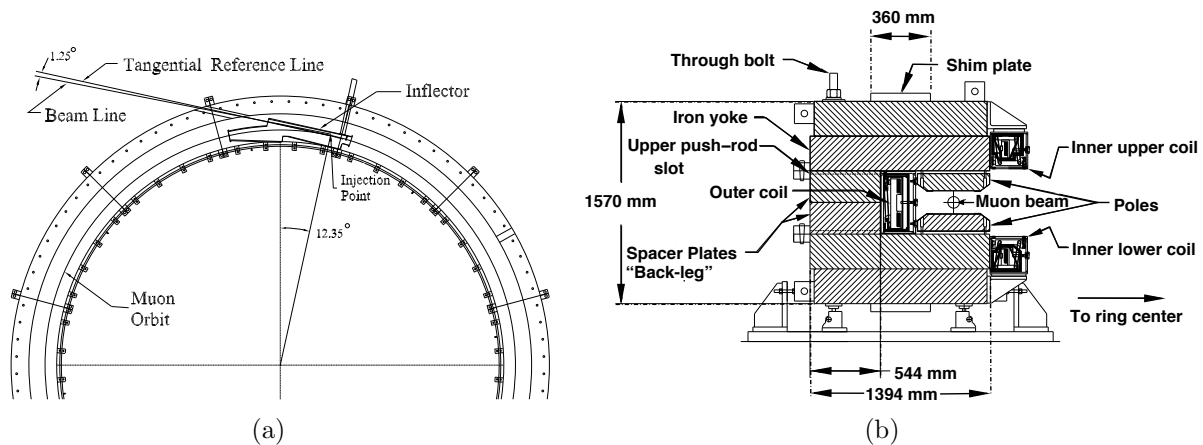


Figure 3.2: (a) Plan view of the beam entering the storage ring. (b) Elevation view of the storage-ring magnet cross section.

The beam enters through a hole in the “back-leg” of the magnet and then crosses into the inflector magnet, which provides an almost field free region, delivering the beam to the edge of the storage region. The geometry is rather constrained, as can be seen in Fig. 3.3(a). The injection geometry is sketched in Fig. 3.3(b). The kick required to put magic momentum muons onto a stable orbit centered at magic radius is on the order of 10 mrad.

The requirements on the muon kicker are rather severe:

1. Since the magnet is continuous, any kicker device has to be inside of the precision magnetic field region.
2. The kicker hardware cannot contain magnetic elements such as ferrites, because they will spoil the uniform magnetic field.
3. Any eddy currents produced in the vacuum chamber, or in the kicker electrodes by the kicker pulse must be negligible by 10 to 20 μs after injection, or must be well known and corrected for in the measurement.
4. Any new kicker hardware must fit within the real estate that was occupied by the E821 kicker. The available space consists of three consecutive 1.7 m long spaces; see Fig. 3.5

5. The kicker pulse should be shorter than the cyclotron period of 149 ns.

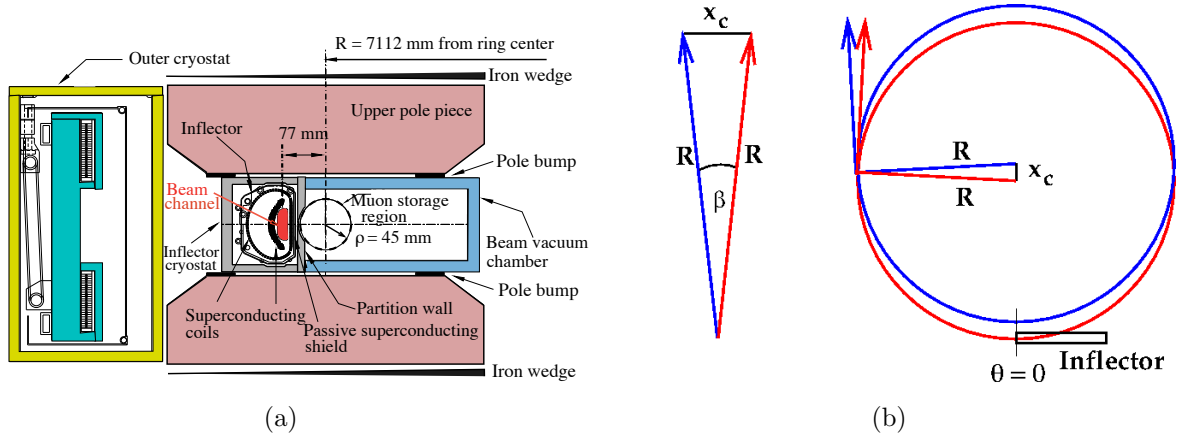


Figure 3.3: (a) The inflector exit showing the incident beam center 77 mm from the center of the storage region. The incident muon beam channel is highlighted in red. (b) The geometry of the necessary kick. The incident beam is the red circle, and the kick effectively moves the red circle over to the blue one.

3.3 The Spin Equations

Measurements of magnetic and electric dipole moments make use of the torque on a dipole in an external field:

$$\vec{\tau} = \vec{\mu} \times \vec{B} + \vec{d} \times \vec{E}, \quad (3.3)$$

where we include the possibility of an electric dipole moment (\vec{d}). Except for the original Nevis spin rotation experiment, the muon magnetic dipole moment experiments inject a beam of polarized muons into a magnetic field and measure the rate at which the spin turns relative to the momentum, $\vec{\omega}_a = \vec{\omega}_S - \vec{\omega}_C$, where S and C stand for spin and cyclotron, respectively. These two frequencies, in the absence of any other external fields, are given by

$$\omega_S = -g \frac{Qe}{2m} B - (1 - \gamma) \frac{Qe}{\gamma m} B; \quad (3.4)$$

$$\omega_C = -\frac{Qe}{m\gamma} B; \quad (3.5)$$

$$\omega_a = \omega_S - \omega_C = -\left(\frac{g-2}{2}\right) \frac{Qe}{m} B = -a_\mu \frac{Qe}{m} B \quad (3.6)$$

(where $e > 0$ and $Q = \pm 1$). There are two important features of ω_a :

- It only depends on the anomaly rather than on the full magnetic moment.
- It depends linearly on the applied magnetic field.

To measure the anomaly, it is necessary to measure ω_a , and to determine the magnetic field B . The relevant quantity is $\langle B \rangle$, which is the magnetic field convolved with the muon beam distribution,

$$\langle B \rangle = \int M(r, \theta) B(r, \theta) r dr d\theta, \quad (3.7)$$

where the magnetic field $B(r, \theta)$ is expressed in terms of a multipole expansion

$$B(r, \theta) = \sum_{n=0}^{\infty} r^n [c_n \cos n\theta + s_n \sin n\theta], \quad (3.8)$$

and the muon distribution is expressed in terms of moments

$$M(r, \theta) = \sum_{m=0}^{\infty} [\xi_m(r) \cos m\theta + \sigma_m(r) \sin m\theta]. \quad (3.9)$$

Because the harmonics $\sin n\theta \sin m\theta$, etc., are orthogonal and vanish for $m \neq n$ when integrated over one period, non-vanishing integrals come from products of the same moment/multipole, in the expression for $\langle B \rangle$. To determine $\langle B \rangle$ to sub-part-per-million (ppm) precision, one either needs excellent knowledge of the multipole and moment distributions for B and M ; or care must be taken to minimize the number of terms, with only the leading term being large, so that only the first few multipoles are important. This was achieved in the most recent experiment [1] by using a circular beam aperture, and making a very uniform dipole magnetic field.

However there is one important issue to be solved: How can the muon beam be confined to a storage ring if significant magnetic gradients cannot be used to provide vertical focusing? The answer to this question was discovered by the third CERN collaboration [2], which used an electric quadrupole field to provide vertical focusing. Of course, a relativistic particle feels a motional magnetic field proportional to $\vec{\beta} \times \vec{E}$, but the full relativistic spin equation contains a cancellation as can be seen below. Assuming that the velocity is transverse to the magnetic field ($\vec{\beta} \cdot \vec{B} = 0$), one obtains [3, 4]

$$\vec{\omega}_a = -\frac{Qe}{m} \left[a_\mu \vec{B} - \left(a_\mu - \left(\frac{mc}{p} \right)^2 \right) \frac{\vec{\beta} \times \vec{E}}{c} \right] = -\frac{Qe}{m} \left[a_\mu \vec{B} - \left(a_\mu - \frac{1}{\gamma^2 - 1} \right) \frac{\vec{\beta} \times \vec{E}}{c} \right]. \quad (3.10)$$

For the “magic” momentum $p_{\text{magic}} = m/\sqrt{a} \simeq 3.09 \text{ GeV}/c$ ($\gamma_{\text{magic}} = 29.3$), the second term vanishes, and the electric field does not contribute to the spin motion *relative* to the momentum.² If $g = 2$, then $a_\mu = 0$ and the spin would follow the momentum, turning at the cyclotron frequency.

If an electric dipole moment were to be present (see Eq. 2.4), it would modify the spin equation to

$$\vec{\omega}_{a\eta} = \vec{\omega}_a + \vec{\omega}_\eta = -\frac{Qe}{m} \left[a \vec{B} - \left(a - \frac{1}{\gamma^2 - 1} \right) \frac{\vec{\beta} \times \vec{E}}{c} \right] - \eta \frac{Qe}{2m} \left[\frac{\vec{E}}{c} + \vec{\beta} \times \vec{B} \right] \quad (3.11)$$

²Small corrections to the measured frequency must be applied since $\vec{\beta} \cdot \vec{B} \simeq 0$ and not all muons are at the magic momentum. These are discussed in Chapter 4.

where η plays the same role for the EDM as g plays for the MDM.

To good approximation, ω_a is directed parallel to the \vec{B} field, and ω_η is directed radially since the motional electric field proportional to $\vec{\beta} \times \vec{B}$ dominates over the quadrupole electric field. The net effects of the EDM are to tip the plane of polarization precession out of the ring plane by the angle $\delta = \tan^{-1} \frac{\eta\beta}{2a_\mu}$ (see Fig. 3.4), and to increase the magnitude of the precession according to $\omega = \sqrt{\omega_a^2 + \omega_\eta^2} = \sqrt{\omega_a^2 + \left(\frac{e\eta\beta B}{2m}\right)^2}$. This tipping causes the average vertical component of the momentum of the decay positrons to oscillate with frequency ω_a , but out of phase with the number oscillation (Eq. 3.18) by $\pi/2$.

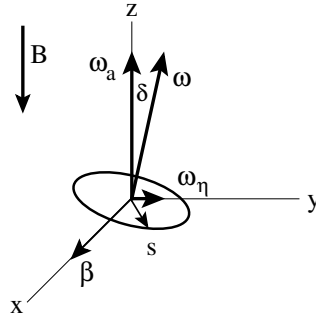


Figure 3.4: (b) The vectors $\vec{\omega}_a$ and $\vec{\omega}_\eta$ showing the tipping of the precession plane because of the presence of an electric dipole moment.

Since E989 will be equipped with three tracking stations that are useful for determining the properties of the stored muon beam, the up-down oscillating EDM signal comes for free. E989 should be able to improve on the E821 muon EDM limit [5] of

$$d_\mu < 1.8 \times 10^{-19} e \cdot \text{cm} \quad (95\% \text{C.L.}) \quad (3.12)$$

two or more orders of magnitude. The most recent measurement of the electron EDM obtained [6] $d_e < 8.7 \times 10^{-29} e \cdot \text{cm}$ (90% C.L.). While a naive scaling between the electron and muon EDM goes linearly with mass, there are SUSY models that predict a much larger scaling [7].

3.4 Vertical Focusing with Electrostatic Quadrupoles

The storage ring acts as a weak-focusing betatron, with the vertical focusing provided by electrostatic quadrupoles. The ring is operated at the magic momentum, so that the electric field does not contribute to the spin precession. However there is a second-order correction to the spin frequency from the radial electric field, which is discussed below. There is also a correction from the vertical betatron motion, since the spin equations in the previous section were derived with the assumption that $\vec{\beta} \cdot \vec{B} = 0$.

A pure quadrupole electric field provides a linear restoring force in the vertical direction, and the combination of the (defocusing) electric field and the central (dipole) magnetic field

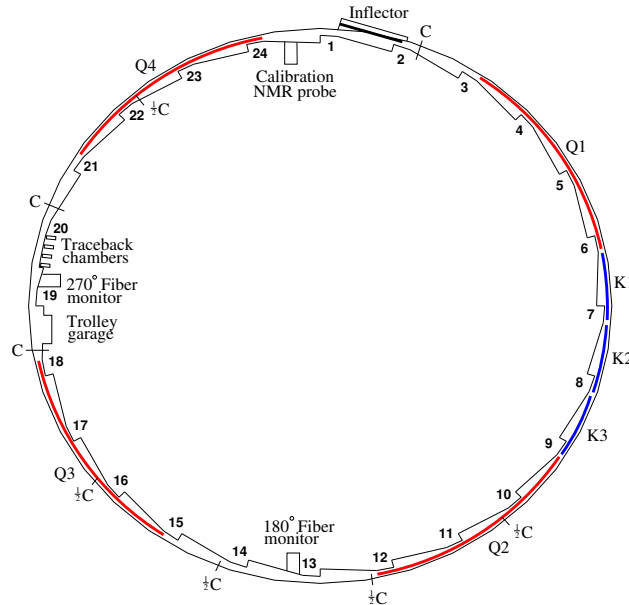


Figure 3.5: The layout of the storage ring, as seen from above, showing the location of the inflector, the kicker sections (labeled K1-K3), and the quadrupoles (labeled Q1-Q4). The beam circulates in a clockwise direction. Also shown are the collimators, which are labeled “C”, or “ $\frac{1}{2}C$ ” indicating whether the Cu collimator covers the full aperture, or half the aperture. The collimators are rings with inner radius: 45 mm, outer radius: 55 mm, thickness: 3 mm. The scalloped vacuum chamber consists of 12 sections joined by bellows. The chambers containing the inflector, the NMR trolley garage, and the trolley drive mechanism are special chambers. The other chambers are standard, with either quadrupole or kicker assemblies installed inside. An electron calorimeter is placed behind each of the radial windows, at the position indicated by the calorimeter number.

(B_0) provides a net linear restoring force in the radial direction. The important parameter is the field index, n , which is defined by

$$n = \frac{\kappa R_0}{\beta B_0}, \quad (3.13)$$

where κ is the electric quadrupole gradient and R_0 is the storage ring radius. For a ring with a uniform vertical dipole magnetic field and a uniform quadrupole field that provides vertical focusing covering the full azimuth, the stored particles undergo simple harmonic motion called betatron oscillations, in both the radial and vertical dimensions. The beam motion is discussed in more detail in the following chapter.

3.5 Muon Decay

The dominant muon decay is

$$\mu^\mp \rightarrow e^\mp + \nu_\mu(\bar{\nu}_\mu) + \bar{\nu}_e(\nu_e) \quad (3.14)$$

which also violates parity.

Since the kinematics of muon decay are central to the measurements of a_μ , we discuss the general features in this section. Additional details are given in Ref. [8]. From a beam of pions traversing a straight beam-channel consisting of focusing and defocusing elements (FODO), a beam of polarized, high energy muons can be produced by selecting the "forward" or "backward" decays. The forward muons are those produced, in the pion rest frame, nearly parallel to the pion laboratory momentum and are the decay muons with the highest laboratory momenta. The backward muons are those produced nearly anti-parallel to the pion momentum and have the lowest laboratory momenta. The forward μ^- (μ^+) are polarized along (opposite) their lab momenta respectively; the polarization reverses for backward muons. The E821 experiment used forward muons, as will E989, the difference being the length of the pion decay line, which in E989 will be 1,900 m, compared with 80 m in E821.

The pure $(V - A)$ three-body weak decay of the muon, $\mu^- \rightarrow e^- + \nu_\mu + \bar{\nu}_e$ or $\mu^+ \rightarrow e^+ + \bar{\nu}_\mu + \nu_e$, is "self-analyzing", that is, the parity-violating correlation between the directions in the muon rest frame (MRF) of the decay electron and the muon spin can provide information on the muon spin orientation at the time of the decay. When the decay electron has the maximum allowed energy in the MRF, $E'_{\max} \approx (m_\mu c^2)/2 = 53$ MeV, the neutrino and anti-neutrino are directed parallel to each other and at 180° relative to the electron direction. The $\nu\bar{\nu}$ pair carry zero total angular momentum; the electron carries the muon's angular momentum of $1/2$. The electron, being a lepton, is preferentially emitted left-handed in a weak decay, and thus has a larger probability to be emitted with its momentum *anti-parallel* rather than parallel to the μ^- spin. Similarly, in μ^+ decay, the highest-energy positrons are emitted *parallel* to the muon spin in the MRF.

In the other extreme, when the electron kinetic energy approaches zero in the MRF, the neutrino and anti-neutrino are emitted back-to-back and carry a total angular momentum of one. In this case, the electron spin is directed opposite to the muon spin in order to conserve angular momentum. Again, the electron is preferentially emitted with helicity -1; however, in this case its momentum will be preferentially directed *parallel* to the μ^- spin. The positron, in μ^+ decay, is preferentially emitted with helicity +1, and therefore its momentum will be preferentially directed *anti-parallel* to the μ^+ spin.

With the approximation that the energy of the decay electron $E' \gg m_e c^2$, the differential decay distribution in the muon rest frame is given by[9],

$$dP(y', \theta') \propto n'(y') [1 \pm \mathcal{A}(y') \cos \theta'] dy' d\Omega' \quad (3.15)$$

where y' is the momentum fraction of the electron, $y' = p'_e/p'_{e \max}$, $d\Omega'$ is the solid angle, $\theta' = \cos^{-1}(\hat{p}'_e \cdot \hat{s})$ is the angle between the muon spin \hat{s} and \hat{p}'_e , $p'_{e \max} c \approx E'_{\max}$, and the $(-)$ sign is for negative muon decay. The number distribution $n(y')$ and the decay asymmetry $\mathcal{A}(y')$ are given by

$$n(y') = 2y'^2(3 - 2y') \quad \text{and} \quad \mathcal{A}(y') = \frac{2y' - 1}{3 - 2y'}. \quad (3.16)$$

Note that both the number and asymmetry reach their maxima at $y' = 1$, and the asymmetry changes sign at $y' = \frac{1}{2}$, as shown in Figure 3.6(a).

The CERN and Brookhaven based muon ($g - 2$) experiments stored relativistic muons of the magic momentum in a uniform magnetic field, which resulted in the muon spin precessing

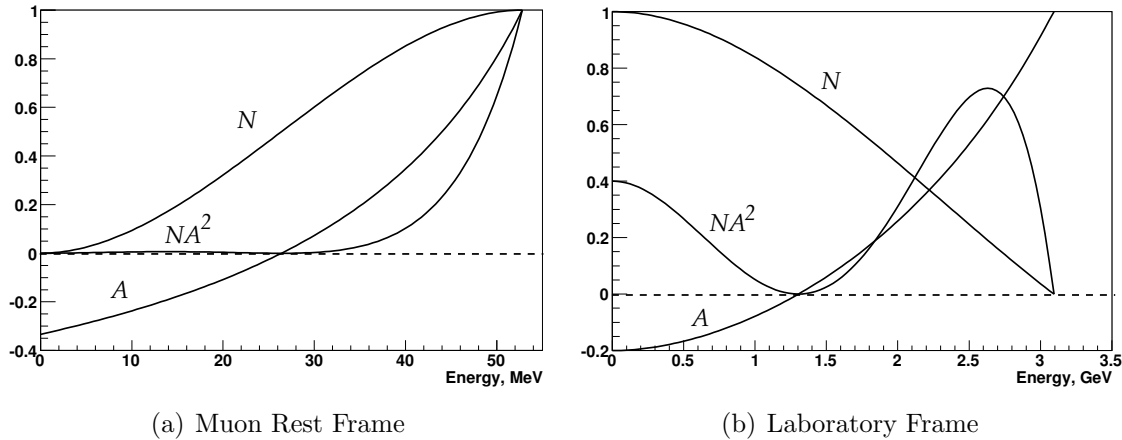


Figure 3.6: Number of decay electrons per unit energy, N (arbitrary units), value of the asymmetry A , and relative figure of merit NA^2 (arbitrary units) as a function of electron energy. Detector acceptance has not been incorporated, and the polarization is unity. For the third CERN experiment and E821, $E_{max} \approx 3.1$ GeV ($p_\mu = 3.094$ GeV/c) in the laboratory frame.

with constant frequency $\vec{\omega}_a$, while the muons traveled in circular orbits. If *all* decay electrons were counted, the number detected as a function of time would be a pure exponential; therefore we seek cuts on the laboratory observable to select subsets of decay electrons whose numbers oscillate at the precession frequency. The number of decay electrons in the MRF varies with the angle between the electron and spin directions, the electrons in the subset should have a preferred direction in the MRF when weighted according to their asymmetry as given in Equation 3.15. At $p_\mu \approx 3.094$ GeV/c the directions of the electrons resulting from muon decay in the laboratory frame are very nearly parallel to the muon momentum regardless of their energy or direction in the MRF. The only practical remaining cut is on the electron's laboratory energy. An energy subset will have the desired property: there will be a net component of electron MRF momentum either parallel or antiparallel to the laboratory muon direction. For example, suppose that we only count electrons with the highest laboratory energy, around 3.1 GeV. Let \hat{z} indicate the direction of the muon laboratory momentum. The highest-energy electrons in the laboratory are those near the maximum MRF energy of 53 MeV, and with MRF directions nearly parallel to \hat{z} . There are more of these high-energy electrons when the μ^- spins are in the direction opposite to \hat{z} than when the spins are parallel to \hat{z} . Thus the number of decay electrons reaches a maximum when the muon spin direction is opposite to \hat{z} , and a minimum when they are parallel. As the spin precesses the number of high-energy electrons will oscillate with frequency ω_a . More generally, at laboratory energies above ~ 1.2 GeV, the electrons have a preferred average MRF direction parallel to \hat{z} (see Figure 3.6). In this discussion, it is assumed that the spin precession vector, $\vec{\omega}_a$, is independent of time, and therefore the angle between the spin component in the orbit plane and the muon momentum direction is given by $\omega_a t + \phi$, where ϕ is a constant.

Equations 3.15 and 3.16 can be transformed to the laboratory frame to give the electron

number oscillation with time as a function of electron energy,

$$N_d(t, E) = N_{d0}(E)e^{-t/\gamma\tau}[1 + A_d(E) \cos(\omega_a t + \phi_d(E))], \quad (3.17)$$

or, taking all electrons above threshold energy E_{th} ,

$$N(t, E_{th}) = N_0(E_{th})e^{-t/\gamma\tau}[1 + A(E_{th}) \cos(\omega_a t + \phi(E_{th}))]. \quad (3.18)$$

In Equation 3.17 the differential quantities are,

$$A_d(E) = \mathcal{P} \frac{-8y^2 + y + 1}{4y^2 - 5y - 5}, \quad N_{d0}(E) \propto (y - 1)(4y^2 - 5y - 5), \quad (3.19)$$

and in Equation 3.18,

$$N(E_{th}) \propto (y_{th} - 1)^2(-y_{th}^2 + y_{th} + 3), \quad A(E_{th}) = \mathcal{P} \frac{y_{th}(2y_{th} + 1)}{-y_{th}^2 + y_{th} + 3}. \quad (3.20)$$

In the above equations, $y = E/E_{max}$, $y_{th} = E_{th}/E_{max}$, \mathcal{P} is the polarization of the muon beam, and E , E_{th} , and $E_{max} = 3.1$ GeV are the electron laboratory energy, threshold energy, and maximum energy, respectively.

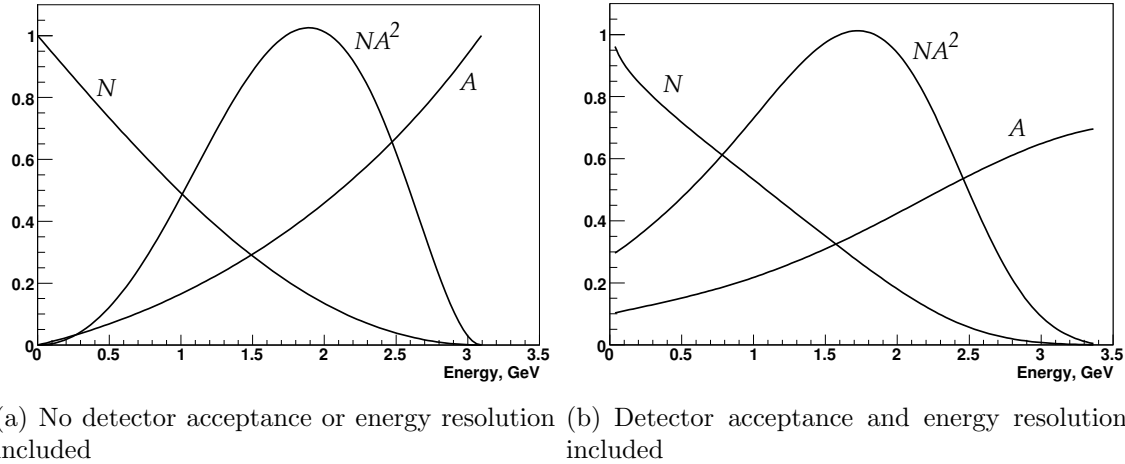


Figure 3.7: The integral N , A , and NA^2 (arbitrary units) for a single energy-threshold as a function of the threshold energy; (a) in the laboratory frame, not including and (b) including the effects of detector acceptance and energy resolution for the E821 calorimeters. For the third CERN experiment and E821, $E_{max} \approx 3.1$ GeV ($p_\mu = 3.094$ GeV/c) in the laboratory frame.

The fractional statistical error on the precession frequency, when fitting data collected over many muon lifetimes to the five-parameter function (Equation 3.18), is given by

$$\delta\epsilon = \frac{\delta\omega_a}{\omega_a} = \frac{\sqrt{2}}{2\pi f_a \tau_\mu \sqrt{NA^2}}. \quad (3.21)$$

where N is the total number of electrons, and A is the asymmetry, in the given data sample. For a fixed magnetic field and muon momentum, the statistical figure of merit is NA^2 , the quantity to be maximized in order to minimize the statistical uncertainty.

The energy dependencies of the numbers and asymmetries used in Equations 3.17 and 3.18, along with the figures of merit NA^2 , are plotted in Figures 3.6 and 3.7 for the case of E821. The statistical power is greatest for electrons at 2.6 GeV (Figure 3.6). When a fit is made to all electrons above a single energy threshold, the optimal threshold energy is about 1.7-1.8 GeV (Figure 3.7).

The resulting arrival-time spectrum of electrons with energy greater than 1.8 GeV from the final E821 data run is shown in Fig. 3.8. While this plot clearly exhibits the expected features of the five-parameter function, a least-square fit to these 3.6 billion events gives an unacceptably large chi-square. A number of small effects must be taken into account to obtain a reasonable fit, which will be discussed in Chapter 5.

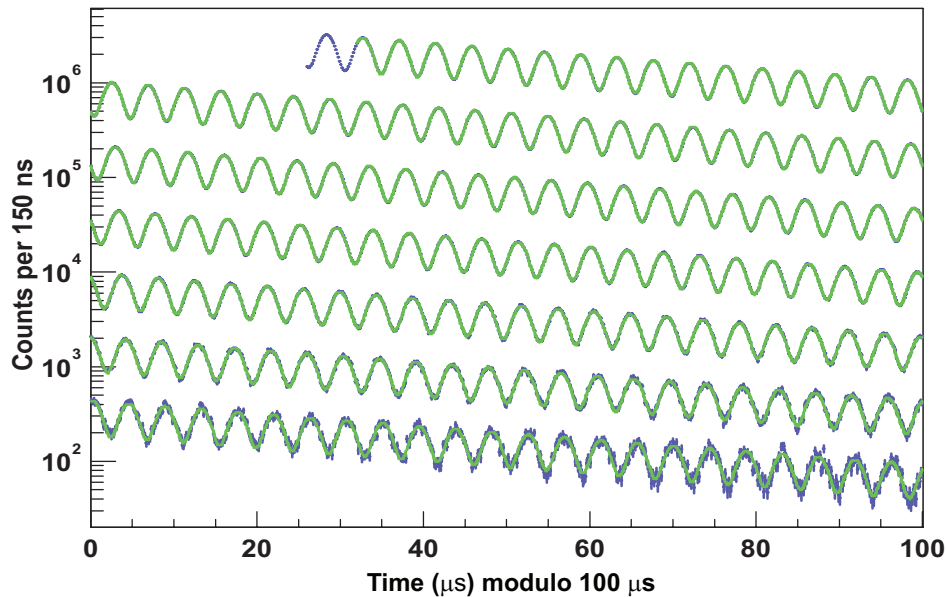


Figure 3.8: Histogram, modulo $100 \mu s$, of the number of detected electrons above 1.8 GeV for the 2001 data set as a function of time, summed over detectors, with a least-squares fit to the spectrum superimposed. Total number of electrons is 3.6×10^9 . The data are in blue, the fit in green.

3.6 The Magnetic Field

The rate at which the muon spin turns relative to its momentum (Eq. 3.10) depends on the anomaly a_μ and on the average magnetic field given by Eq. 3.7. Thus the determination of a_μ to sub-tenths of a ppm requires that both ω_a and $\langle B \rangle$ be determined to this level. The muon beam is confined to a cylindrical region of 9 cm diameter, which is 44.7 m in length. The volume of this region is $\simeq 1.14 \text{ m}^3$ or $\simeq 40 \text{ ft}^3$, which sets the scale for the magnetic field measurement and control. The E989 goal is to know the magnetic field averaged over running time and the muon distribution to an uncertainty of ± 70 parts per billion (ppb).

The problem breaks into several pieces:

1. Producing as uniform magnetic field as possible by shimming the magnet.
2. Stabilizing B in time at the sub-ppm level by feedback, with mechanical and thermal stability.
3. Monitoring B to the 20 ppb level around the storage ring during data collection.
4. Periodically mapping the field throughout the storage region and correlating the field map to the monitoring information without turning off the magnet between data collection and field mapping. It is essential that the magnet not be powered off unless absolutely necessary.
5. Obtaining an absolute calibration of the B -field relative to the Larmor frequency of the free proton.

The only magnetic field measurement technique with the sensitivity needed to measure and control the B -field to the tens of ppb is nuclear magnetic resonance (NMR). As in E821, E989 will implement a pulsed NMR setup. In this configuration a $\pi/2$ RF pulse is used to rotate the proton spin and the resulting free-induction decay (FID) will be detected by a pick-up coil around the sample. The E821 baseline design used the NMR of protons in a water sample with a CuSO_4 additive that shortened the relaxation time, with the probes tuned to operate in a 1.45 T field. When the water evaporated from a few of the probes, the water was replaced with petroleum jelly, which has the added features of a smaller sensitivity to temperature changes and no evaporation.

Special nuclear magnetic resonance (NMR) probes [10, 1] were used in E821 to measure and to monitor the magnetic field during the experimental data collection.³ Three types of probes exist: a spherical water probe that provides the absolute calibration to the free proton; cylindrical probes that monitor the field during data collection, and also in an NMR trolley to map the field; and a smaller spherical probe which can be plunged into the muon storage region by means of a bellows system to transfer the absolute calibration to the trolley probes. A collection of 378 cylindrical probes placed in symmetrically machined grooves on the top and bottom of the muon beam vacuum chamber provide a point-to-point measure of the magnetic field while beam is in the storage ring. Probes at the same azimuthal location but different radii gave information on changes to the quadrupole component of the field at that location.

³The probes are described in Chapter 15

The field mapping trolley contains 17 cylindrical probes arranged in concentric circles as shown in Figure 3.9. At several-day intervals during the running periods, the beam will be turned off, and the field mapping trolley will be driven around the inside of the evacuated beam chamber measuring the magnetic field with each of the 17 trolley probes at 6,000 locations around the ring. One of the resulting E821 field maps, averaged over azimuth, is shown in Figure 3.9(b) for reference.

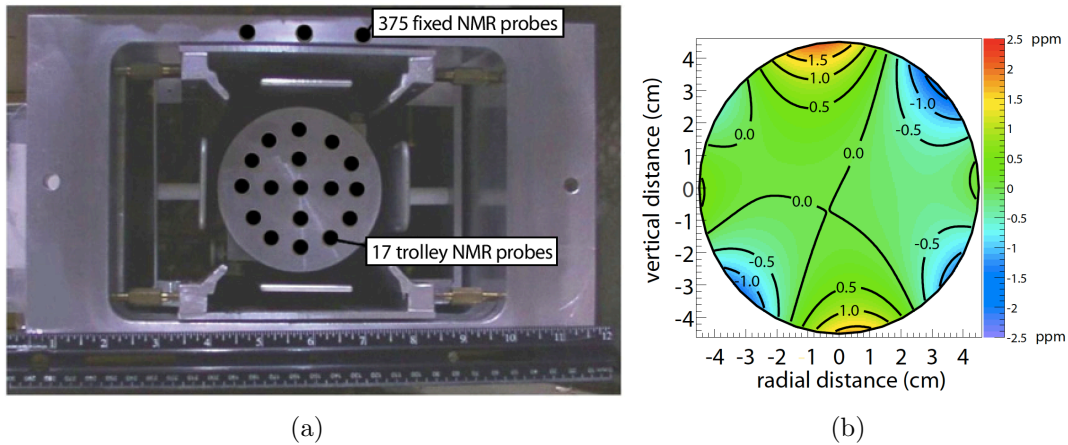


Figure 3.9: (a) The electrostatic quadrupole assembly inside a vacuum chamber showing the NMR trolley sitting on the rails of the cage assembly. Seventeen NMR probes are located just behind the front face in the places indicated by the black circles. The inner (outer) circle of probes has a diameter of 3.5 cm (7 cm) at the probe centers. The storage region has a diameter of 9 cm. The vertical location of three of the 180 upper fixed probes is also shown. An additional 180 probes are located symmetrically below the vacuum chamber. (Reprinted with permission from [1]. Copyright 2006 by the American Physical Society.) (b) A contour plot of the magnetic field averaged over azimuth, 0.5 ppm intervals.

The absolute calibration utilizes a probe with a spherical water sample [11]. The Larmor frequency of a proton in a spherical water sample is related to that of the free proton through $f_L(\text{sph} - \text{H}_2\text{O}, T) = [1 - \sigma(\text{H}_2\text{O}, T)] f_L(\text{free})$, [12, 13] where $\sigma(\text{H}_2\text{O}, 34.7^\circ\text{C}) = 25.790(14) \times 10^{-6}$ is from the diamagnetic shielding of the proton in the water molecule, determined from [14]

$$\sigma(\text{H}_2\text{O}, 34.7^\circ\text{C}) = 1 - \frac{g_p(\text{H}_2\text{O}, 34.7^\circ\text{C})}{g_J(H)} \frac{g_J(H)}{g_p(H)} \frac{g_p(H)}{g_p(\text{free})}. \quad (3.22)$$

The terms are: the ratio of the g -factors of the proton in a spherical water sample to that of the electron in the hydrogen ground state ($g_J(H)$) [14]; the ratio of electron to proton g -factors in hydrogen [15]; the bound-state correction relating the g -factor of the proton bound in hydrogen to the free proton [16, 17]. The temperature dependence is from Reference [18]. An alternate absolute calibration would be to use an optically pumped ^3He NMR probe [19]. This has several advantages: the sensitivity to the probe shape is negligible, and the temperature dependence is also negligible. This option is being explored for E989.

The calibration procedure described above permits the magnetic field to be expressed in terms of the Larmor frequency of a free proton, ω_p . The magnetic field is weighted by the

muon distribution, and also averaged over the running time weighed by the number of stored muons to determine the value of ω_p which is combined with the average ω_a to determine a_μ . The reason for the use of these two frequencies, rather than B measured in tesla can be understood from Eq. 3.10. To obtain a_μ from this relationship requires precise knowledge of the muon charge to mass ratio.

To determine a_μ from the two frequencies ω_a and ω_p , we use the relationship

$$a_\mu = \frac{\omega_a/\omega_p}{\lambda_+ - \omega_a/\omega_p} = \frac{\mathcal{R}}{\lambda_+ - \mathcal{R}}, \quad (3.23)$$

where the ratio

$$\lambda_+ = \mu_{\mu^+}/\mu_p = 3.183\,345\,137\,(85) \quad (3.24)$$

is the muon-to-proton magnetic moment ratio [20] measured from muonium (the μ^+e^- atom) hyperfine structure[21]. Of course, to use λ_+ to determine a_{μ^-} requires the assumption of *CPT* invariance, *viz.* ($a_{\mu^+} = a_{\mu^-}$; $\lambda_+ = \lambda_-$). The comparison of \mathcal{R}_{μ^+} with \mathcal{R}_{μ^-} provides a *CPT* test. In E821

$$\Delta\mathcal{R} = \mathcal{R}_{\mu^-} - \mathcal{R}_{\mu^+} = (3.6 \pm 3.7) \times 10^{-9} \quad (3.25)$$

References

- [1] Bennett GW, et al.(The $g - 2$ Collab.) Phys. Rev. D, 73:072003 (2006)
- [2] J. Bailey, et al., Nucl. Phys. **B150**, 1 (1979).
- [3] L.H. Thomas, Nature **117**, (1926) 514 and Phil. Mag. **3** (1927) 1.
- [4] Bargmann V, Michel L, Telegdi VL, Phys. Rev. Lett. 2:435 (1959)
- [5] G.W. Bennett, et al., (Muon $g-2$ Collaboration) Phys. Rev. **D80** 052008 (2009).
- [6] J. Baron, et al., (ACME Collaboration) Science **343**, 269 (2014)
- [7] K.S. Babu, Bhaskar Dutta, R.N. Mohapatra, Phys. Rev. Lett.**85** (2000) 5064-5067.
- [8] James P. Miller, Eduardo de Rafael and B. Lee Roberts, Rept. Prog. Phys. **70**, 795-881, 2007.
- [9] E.J. Konopinski, Ann. Rev. Nucl. Sci. **9** 99, (1959).
- [10] R. Prigl, *et al.*, Nucl. Inst. Methods Phys. Res. **A374** 118 (1996).
- [11] Fei X, Hughes V, Prigl R, *Nucl. Inst. Methods Phys. Res.* A394:349 (1997)
- [12] Abragam A. In *Principles of Nuclear Magnetism*, p. 173-178. Oxford U. Press, (1961)
- [13] Mohr PJ, Taylor BH, *Rev. Mod. Phys.* 77:1 (2005)
- [14] Phillips WD, et al. *Metrologia* 13:179 (1979)
- [15] Winkler PF, Kleppner D, Myint T, Walther FG, *Phys. Rev.* A5:83 (1972)
- [16] Lamb Jr. WE. *Phys. Rev.* 60:817 (1941)
- [17] Grotch H, Hegstrom RA. *Phys. Rev.* A4:59 (1971)
- [18] B.W. Petley et al. *Metrologia*.**20**, 81 (1984)
- [19] J.L. Flowers, B.W. Petley and M.G. Richards, *Metrologia* **30**, 75 (1993).
- [20] Mohr PJ, Taylor BN, Newell DB, (CODATA recommended values). *Rev. Mod. Phys.* 80:633 (2008)
- [21] W. Liu et al., Phys. Rev. Lett. **82**, 711 (1999).

